

---

# Transport and Separation Characteristics of PVDF-Based Nanocomposite Membranes in Membrane Distillation

---

Syed Farzan Shah , [Naif A. Darwish](#) , [Nabil Abdel Jabbar](#) \* , [Sameer Al-Asheh](#) , Muhammad Qasim , Farouq S. Mjalli

Posted Date: 27 February 2026

doi: 10.20944/preprints202602.1789.v1

Keywords: membrane distillation; carbon nano-tubes; phase inversion; PVDF



Preprints.org is a free multidisciplinary platform providing preprint service that is dedicated to making early versions of research outputs permanently available and citable. Preprints posted at Preprints.org appear in Web of Science, Crossref, Google Scholar, Scilit, Europe PMC.

Copyright: This open access article is published under a [Creative Commons CC BY 4.0 license](#), which permit the free download, distribution, and reuse, provided that the author and preprint are cited in any reuse.

Disclaimer/Publisher's Note: The statements, opinions, and data contained in all publications are solely those of the individual author(s) and contributor(s) and not of MDPI and/or the editor(s). MDPI and/or the editor(s) disclaim responsibility for any injury to people or property resulting from any ideas, methods, instructions, or products referred to in the content.

Article

# Transport and Separation Characteristics of PVDF-Based Nanocomposite Membranes in Membrane Distillation

Syed Farzan Shah <sup>1</sup>, Naif A. Darwish <sup>1</sup>, Nabil Abdel Jabbar <sup>1,\*</sup>, Sameer Al-Asheh <sup>1</sup>,  
Muhammad Qasim <sup>1,2</sup> and Farouq S. Mjalli <sup>3</sup>

<sup>1</sup> Department of Chemical and Biological Engineering, American University of Sharjah, Sharjah, 26666, United Arab Emirates

<sup>2</sup> Materials Science and Engineering Program, College of Arts and Sciences, American University of Sharjah, Sharjah 26666, United Arab Emirates

<sup>3</sup> Petroleum and Chemical Engineering Department, Sultan Qaboos University, Muscat 123, Oman

\* Correspondence: nabdeljabbar@aus.edu

## Abstract

Water scarcity has increased the need for efficient treatment technologies such as membrane distillation (MD). MD performance depends strongly on membrane fabrication parameters, particularly polymer concentration and nanoparticle incorporation, which control key transport and separation properties. This study considers fabrication of membranes using different concentrations of polyvinylidene fluoride (PVDF) with the incorporation of different types of nanoparticles to determine the optimum membrane formulation for membrane distillation applications. The results demonstrate that both PVDF concentration and nanoparticle type play a critical role in membrane performance in terms of permeate flux and salt rejection. Among the nanoparticles studied in this work, carbon nanotubes (CNTs) exhibited the most significant enhancement, leading to a substantial increase in water vapor flux while maintaining excellent separation efficiency. The optimized CNT incorporated membrane achieved approximately 99% salt rejection, with superior flux performance, indicating its strong potential for high-efficiency desalination and water treatment using membrane distillation.

**Keywords:** membrane distillation; carbon nano-tubes; phase inversion; PVDF

## 1. Introduction

Safe and reliable water is essential for health, food production, energy, and economic growth. Only 0.036% of global water is actually accessible for human use, with around 80% of the world's population facing water supply threats [1]. Increasing population, urbanization and climate change make freshwater resources a challenging issue. In addition, pollution from untreated industrial waste, agricultural runoff, and salty water limit the availability of usable freshwater. These problems make it necessary to develop effective and sustainable water treatment and desalination technologies to provide clean water for the future.

As freshwater resources become increasingly limited, seawater offers a promising alternative due to its abundance, Water covers over 70% of Earth's surface, yet an about 97.5% of it is salty water [2]. Through modern desalination technologies, seawater can be converted into safe and potable water, providing a reliable supply for drinking, industrial, and agricultural needs. Utilizing seawater not only helps address water scarcity but also reduces the pressure on natural freshwater sources, making it an important component for management and strategies of sustainable water.

There are several technologies available for treating seawater; these are generally categorized as thermal-based or membrane-based technologies. However, membrane-based technologies are

considered the most efficient and widely used due to their lower energy consumption, high separation efficiency, and ability to produce high-quality water with minimal chemical use [3–5]. Among these, processes such as reverse osmosis, nanofiltration, and membrane distillation depend on selective separation through semi-permeable membranes. In a membrane-based processes, water molecules transport through the membrane while salts and other impurities are retained, allowing for effective purification. The working principle typically depends on either pressure-driven flow, as in reverse osmosis, or thermally driven vapor transport, as in membrane distillation (MD), where a hydrophobic membrane allows only water vapor to pass while rejecting liquid water and dissolved salts [6,7].

MD technology has gained significant attention in recent years as a promising method for seawater desalination and wastewater treatment. Unlike traditional pressure-driven membrane processes, MD is also considered as a thermally driven process that operates at lower pressures and moderate temperatures. This makes it energy-efficient process, especially when integrated with renewable heat sources such as solar or waste heat. This would offer high salt rejection and excellent water quality, even when treating highly saline or contaminated water that makes it challenging compared to other conventional technologies [8]. Furthermore, MD membranes are less prone to fouling and scaling compared to pressure-driven membranes, which extends membrane life and reduces operational costs. These advantages make MD a versatile and sustainable solution for producing clean water in regions facing severe water scarcity or limited access to freshwater resources.

The performance of MD system largely depends on the quality and properties of the membrane used. A high-performing membrane is essential for achieving maximum water flux, high salt rejection, and long-term stability [9]. Key characteristics such as porosity, pore size, thickness, and surface hydrophobicity play critical role in allowing efficient water vapor transport while preventing wetting and fouling. Additionally, mechanical strength and thermal stability are important characteristics to ensure that the membrane can operate reliably under different conditions [10]. Therefore, developing or selecting the best-performing membrane is crucial for optimizing MD efficiency, reducing energy consumption, and maintaining consistent water production over time.

Concentration of polymer plays a vital role in controlling membrane performance, as it strongly affects solution viscosity, phase separation behaviour, and polymer–solvent–nonsolvent interactions during membrane formation. At lower polymer concentrations, rapid mixing can be achieved leading to the formation of highly porous structures with larger pores and finger-like macro-voids. In contrast, increasing the polymer concentration results in delayed phase separation, producing denser membranes with smaller pore sizes, thus reduced porosity, and improved mechanical strength [11,12]. Therefore, careful selection of polymer concentration is essential to tailor membrane morphology and achieve a desirable balance between permeability, selectivity, and structural stability.

In addition to polymer concentration, the incorporation of nanoparticles into membranes has a significant impact on their performance. Nanoparticles can enhance such key properties as porosity, surface roughness, hydrophobicity, and mechanical strength, which are critical for efficient membrane distillation process [13]. Nanoparticles enhance water vapor transport and reduce membrane wetting, thereby increasing water flux while maintaining high salt rejection. [14]. Different types of nanoparticles, such as carbon nanotubes, silica, or metal oxides, can be tailored to improve membrane properties. Therefore, the addition of nanoparticles is a promising strategy to optimize membrane performance and achieve higher efficiency and durability in MD systems.

Membranes can be fabricated by different techniques. Among the various membrane fabrication techniques, Non-Solvent Induced Phase Separation (NIPS) is considered as one of the simplest and most widely used methods. In this technique, a polymer, such as PVDF, is dissolved in a suitable solvent to form a homogeneous solution, which is then cast into a thin film and immersed in a non-solvent bath, typically water [15]. The interaction between the solvent and non-solvent induces polymer precipitation, resulting in the formation of a porous membrane structure. NIPS is widely

used due to its simplicity, cost-effectiveness, and versatility, as it allows precise control over key membrane characteristics such as pore size, porosity, and thickness. These characteristics are typically achieved by variations in polymer concentration, solvent selection, and coagulation conditions, thus making NIPS an effective fabrication method for producing membranes tailored for membrane distillation and other water treatment applications [16,17].

This study considers development of membranes for MD using different polymer concentrations. The optimum membrane was selected based on water flux and salt rejection performance during saline water treatment using direct contact membrane distillation (DCMD) technology. To improve membrane flux, a modified membrane was also developed by incorporating carbon nanotubes (CNTs), graphene oxide (GO), and chitosan as nanofillers. Furthermore, various CNT loadings were examined to identify the optimum CNT concentration that yields the best membrane performance.

## 2. Materials and Methods

All experimental measurements were performed at least twice, and the error were determined from standard error (SE) method and relative error difference percentage. The uncertainties associated with temperature and flow rate measurements were primarily due to instrument resolution and calibration limits. Temperature was measured using a digital thermocouple with an accuracy of  $\pm 0.1$  °C, while the flow rates were controlled by a peristaltic pumps. Mass measurements were carried out using an analytical balance with a readability of  $\pm 0.1$  g.

### 2.1. Materials

All chemicals used in this work were of analytical grade and used without further purification. Polyvinyl difluorides (PVDF MW 534000) as polymer, Multiwalled carbon nano-tubes (50-90 nm diameter, 95% carbon basis), Graphene oxide (0.5-10  $\mu\text{m}$  size, industrial grade, 97% purity), and Chitosan (low MW) were supplied by Sigma-Aldrich, France. N-Methyl-2-pyrrolidone (extra pure AR, 99%) was supplied by Sisco Research Laboratories, India. Sodium chloride (Hi-AR ASSAY 98.5-102%) was supplied by HiMedia Laboratories.

The morphology of the membrane were examined using scanning electron microscope SEM (FE-SEM, TESCAN-MAGNA, Czech Republic). Prior to SEM analysis, the membrane samples were attached onto a sample holder by carbon tape. The samples were then coated with a thin layer of gold using sputter coater (SC7620, Quorum, United Kingdom) machine to enhance its electronic conductivity during sample analysis. The morphology of membrane was observed based on the SEM image using ImageJ (Imagej.Net) software. The hydrophobicity/hydrophilicity of the membrane was measured using the contact angle goniometer device (DSA100M, Kruss GmbH, Germany). In this case, two membrane samples were attached to a glass sheet and placed on the testing plate. Five  $\mu\text{L}$  droplet was placed on the surface of the membrane, and the contact angle was then measured.

### 2.2. Membrane Preparation

#### 2.2.1. Preparation of PVDF Solution

The hydrophobic flat-sheet membranes were prepared. In case of nano-particles present, they were first dispersed in N-Methyl-2-pyrrolidone (NMP) for 1 h using ultrasonication until formation of uniform dispersion. After ultrasonication, PVDF was gradually added to the solvent while continuously heating and stirring for 6 h at 50 °C. The resulting dope solution was left undisturbed to allow removal of any trapped air molecules, and the solution was allowed cool to room temperature.

### 2.2.2. Preparation of Flat Sheet Membrane Using Phase Inversion

Polymeric membranes are typically fabricated using the phase inversion process. A typical phase-inversion fabrication set-up consists of a precision casting head or doctor-blade assembly, a flat and level casting table and moving rod. In this process a polymer solution changes from a liquid phase to a solid phase. Before the formation of the solid phase, a liquid-liquid separation takes place, causing the polymer solution to split into two phases: one with a higher polymer content and the other with less polymer content. The phase with more polymer content can then be solidified to form the membrane structure using gelation or crystallization [18]. The polymer-poor phase creates pores in the solid membrane structure. The process known as immersion precipitation, or nonsolvent induced phase separation (NIPS), require placing the polymer solution into a nonsolvent bath. For this process, the polymer must be soluble in a solvent or solvent mixture, allowing a variety of polymers to be used in membrane synthesis.

The homogeneous polymer solution was poured onto a substrate, such as a glass plate or polymeric support, and spread with a casting knife to create a uniform layer. Each membrane had a thickness of around 150  $\mu\text{m}$  controlled by an adjustable casting knife. This setup enables precise control over film formation, ensuring consistent thickness and a reproducible surface structure. After that, the glass plate was immediately dipped into a coagulation bath, where the solvent and nonsolvent start to exchange. After some time, the membrane solidified and floated to the top of the bath. The programmable film coater as apparatus used for phase inversion process which was supplied by TMAXCN.

## 2.3. Membrane Characterization

### 2.3.1. Membrane Morphology

Morphology provides information about images that reveal the dense skin layer and changes in membrane's porosity at different polymer concentrations [19,20]. SEM can confirm the successful incorporation of additives into the membrane structure, such as CNT or graphene oxide in polyamide layers, enhancing hydrophobic properties and water permeability [21]. In this study, the samples were fixed onto the sample plate using conductive adhesive, completely dried under vacuum, and then coated with a layer of gold.

### 2.3.2. Hydrophobicity/Hydrophilicity

Hydrophilicity and hydrophobicity are key surface features of membranes. Hydrophilic membranes easily attract water and allow higher water flow. Hydrophobic membranes prevent water wetting and are mainly used in vapor separation processes. These surface properties greatly influence membrane performance.

### 2.3.3. Mean Pore Size Calculation

The average pore size of the developed membranes was evaluated using SEM images processed in ImageJ software (ImageJ.Net). Pore diameters were measured at several randomly selected regions on each membrane surface to obtain representative values. For each sample, at least 15 pores were considered, and the mean pore size was calculated. This method allowed for a reliable assessment of membrane morphology and its relevance to separation performance [22].

### 2.3.4. Porosity

The membrane porosity,  $\epsilon$ , was determined by gravitational method which is based on the ratio of the pore volume to the net volume of the porous membrane [23,24]. For each membrane sample, the dry membrane was first weighted ( $m_d$ ), followed by the immersion of the membrane in isopropanol for 2h. According to this method, the porosity can be calculated using the following equation:

$$\varepsilon = \frac{\frac{m_w - m_d}{\rho_i}}{\frac{m_w - m_d}{\rho_i} + \frac{m_d}{\rho_p}} \times 100 \quad (1)$$

where  $m_w$  and  $m_d$  are the mass of wet and dry membrane (kg), respectively,  $\rho_i$  is the density of isopropanol and  $\rho_p$  is the density of polymer. The numerator of above equation represents the pore volume, while the denominator represents the net membrane volume. This was done because isopropanol readily enters and fills the pores, allowing the difference between dry and wet weight with a known density to be used to accurately calculate porosity [25].

### 2.3.5. Water Flux

A lab-scale DCMD setup was used to evaluate the desalination performance using the membranes developed in this work. A piece of the membrane was placed between two pads in a module. The feed solution (salty water 35 g/mL) at high-temperature of 60 °C and the low-temperature permeate solution (DI water at 20-25 °C) were circulated using two peristaltic pumps. The amount of water that overflowed ( $\Delta m$ ), in kg, from the permeate side was measured after a specific time interval ( $\Delta t$ ) to calculate the flux using the following equation:

$$J_w = \frac{\Delta m}{A \times \Delta t} \quad (2)$$

where  $A$  is the cross-sectional area of membrane in  $m^2$ .

### 2.3.6. Salt Rejection

The salt rejection efficiency of the membranes was evaluated by measuring the salt concentration in the feed and permeate solutions, using saline wastewater of known initial concentration as the feed. The salt rejection in both streams was measured by the TDS analyser (HI2003-edge, HANNA). The salt rejection ( $R$ ) percentage was calculated using the following equation [26]:

$$R = \left(1 - \frac{C_p}{C_f}\right) \times 100 \quad (3)$$

## 2.4. Direct Contact Membrane Distillation Set-up

A schematic of the experimental direct contact membrane distillation (DCMD) setup used in this study is shown in Figure 1. In this set-up, a flat-sheet membrane module made of acrylic with an effective area of 0.0021  $m^2$  was used. A fresh membrane was used for each experiment. The feed and permeate streams were pumped at co-current pattern using two peristaltic pumps. The feed temperature and flow rates were varied for each run, while the permeate temperature and flow rates were maintained at about 22 °C and 100 mL/min, respectively, throughout all experiments. The temperature of the permeate side was controlled using an external condenser. Initially, deionized (DI) water was filled into the permeate side graduated tank, which was placed on an electronic balance with an accuracy of 0.1 g. The mass of water transferred was determined from the difference between initial and final readings of the balance. A TDS meter was used to measure the solution's salt rejection in the permeate tank. The hot feed solution was initially placed in a feed tank stirred using a magnetic stirrer. Temperature probes, with an accuracy of  $\pm 0.1$  °C, was used to monitor the temperatures of both streams at the inlets and outlets of the membrane module.

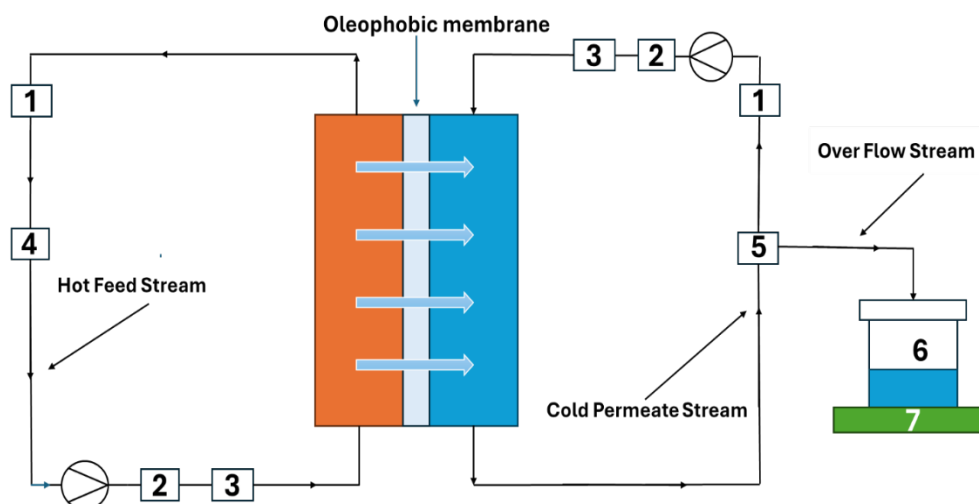


**Figure 1.** Schematic diagram of the DCMD setup: (1) conductivity meter; (2) flow transmitter; (3) temperature transmitter; (4) heater; (5) cooler; (6) product water collection tank; (7) balance.

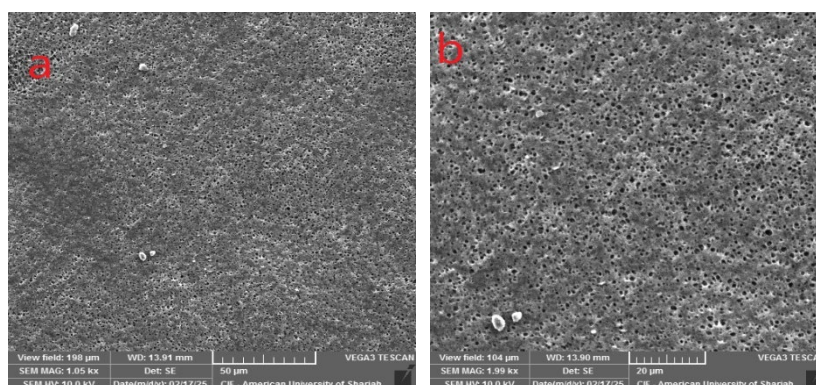
### 3. Results and Discussion

#### 3.1. PVDF Membrane Characterization

##### 3.1.1. SEM Images and Pore Size Distribution

PVDF membranes prepared under identical fabrication conditions but with different polymer concentrations, namely 13-wt% and 20-wt%, exhibited distinct surface morphologies. The SEM images are shown in Figure 2 at different magnifications. At 20  $\mu\text{m}$  magnification, the 20-wt% PVDF membrane cast reveals a denser surface (Figure 2c) with reduced pore size, while the 13-wt% PVDF membrane (Figure 2b) reveals a more open and porous structure. This difference can be attributed to the increase in polymer content that enhances dope viscosity, thus reducing the rate of solvent-nonsolvent exchange during phase inversion [27,28]. Consequently, higher polymer loading results in delayed demixing and formation of a compact surface layer.

The pore size distribution is shown in Figure 3. It can be said that both membranes show almost equally pore size distribution. However, the average pore size of 20%-PVDF- membrane was decreased compared to that of 13%-PVDF. This is because the polymer-rich phase dominates earlier during phase separation, limiting the growth of polymer-lean (pore-forming) regions [29]. At the same time, the pore formation kinetics can be dominated by diffusion-limited processes rather than rapid demixing, which tends to stabilize the pore size distribution. This indicates that the pore size might decrease further only slowly and the variation in pore diameters narrows [30].



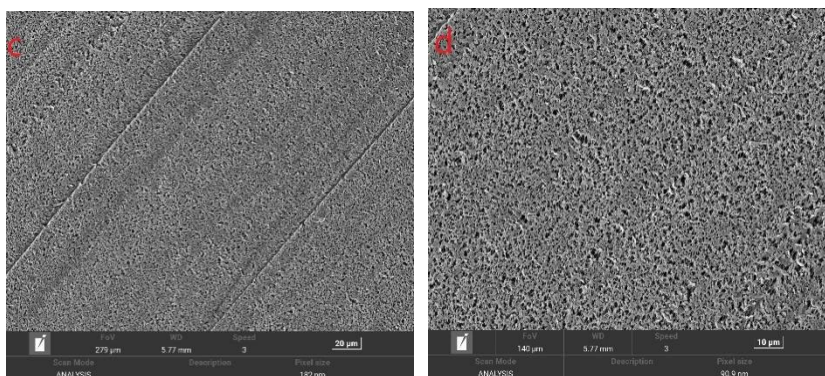


**Figure 2.** SEM images of the membrane at different PVDF concentrations and different magnifications: (a) 13-wt% PVDF at 50  $\mu\text{m}$ ; (b) 13-wt% PVDF at 20  $\mu\text{m}$ ; (c) 20-wt% PVDF at 20  $\mu\text{m}$ ; (d) 20-wt% PVDF at 10  $\mu\text{m}$ .

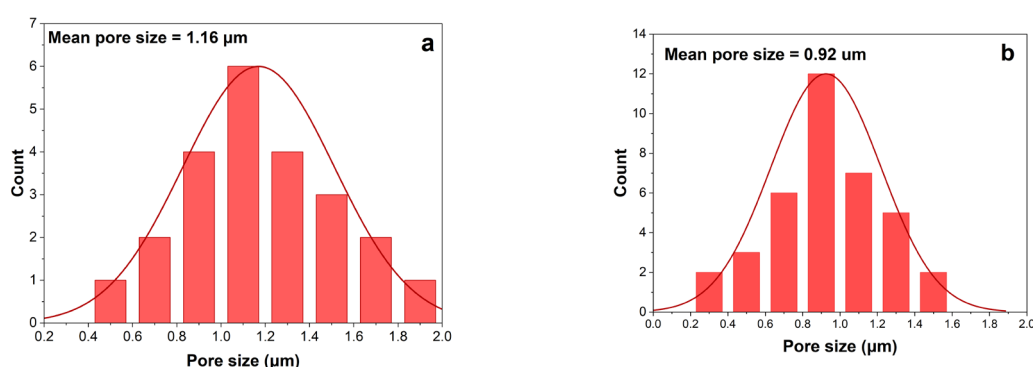


**Figure 3.** Pore size distribution of membrane at different PVDF concentration: (a) 13-wt% PVDF; (b) 20-wt% PVDF.

The SEM images revealed that the pores appear blurred or partially covered upon adding nanoparticles in the membranes (Figure 4). The SEM images for 13%-PVDF-0.5-wt% CNT and 13%-PVDF-0.7-wt% CNT images captured at 20  $\mu\text{m}$  and 5  $\mu\text{m}$ , respectively, showed that increasing CNT concentration causes the pores blurred or partially covered (Figure 4b and c). This is mainly due to the interaction between the CNT additives and the PVDF matrix, which alters the solvent–nonsolvent exchange rate and increases solution viscosity. For CNT particles, it is expected that their high surface area and strong polymer interaction reduce demixing in localized regions, resulting in a smoother and denser appearance [31].

Figure 4e and display the morphology of the membrane containing 0.5-wt% GO. Relative to CNTs, the membrane shows a denser top layer due to the two-dimensional nanosheet structure and high specific surface area of GO. At low concentrations, these sheets can overlap, creating a structure that is highly extended relative to its mass. It has been reported that GO increased the accelerated phase change, producing a thin but compact top layer [32].

The images presented in Figure 4g and h show that chitosan was poorly dispersed in the PVDF - NMP casting solution. This is due to the inherently hydrophilic nature of chitosan, whereas PVDF is strongly hydrophobic, which limits their miscibility in a common casting solution. Poor compatibility can lead to aggregation, resulting in visible surface of chitosan particles.

The pore size distributions of 0.5-wt % CNT and 0.7-wt % CNT are shown in Figure 5. The 0.5-wt % CNT membrane shows a more uniform pore size distribution compared to the 0.7-wt % CNT. Although the difference was very small, the multiwalled nature of CNTs made the blending process more difficult, resulting in an uneven pore distribution in the membrane [26,33]. Figure 4 d shows that some areas with larger pores while others remain denser, resulting in a non-uniform pore structure.

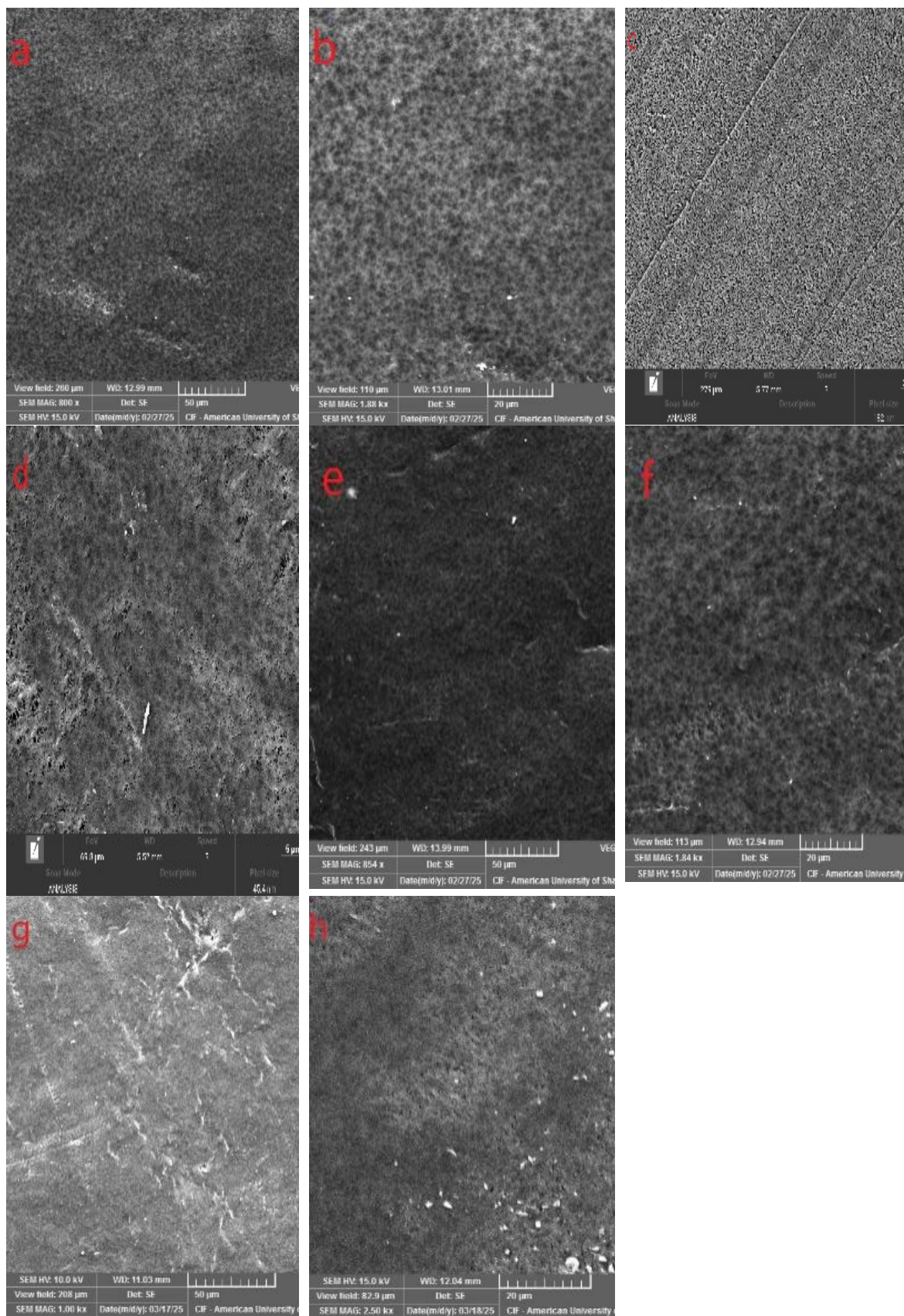


**Figure 4.** SEM images of the membranes with different additives: (a) PVDF-0.5-wt% CNT at 50  $\mu\text{m}$ ; (b) PVDF-0.5-wt% CNT at 20  $\mu\text{m}$ ; (c) PVDF-0.7-wt% CNT at 5  $\mu\text{m}$ ; (d) PVDF-0.7-wt% CNT at 5  $\mu\text{m}$ ; (e) PVDF-0.5-wt% GO at 50  $\mu\text{m}$ ; (f) PVDF-0.5-wt% GO at 20  $\mu\text{m}$ ; (g) PVDF-0.5-wt% CH at 50  $\mu\text{m}$ ; (h) PVDF-0.5-wt% CH at 20  $\mu\text{m}$ .

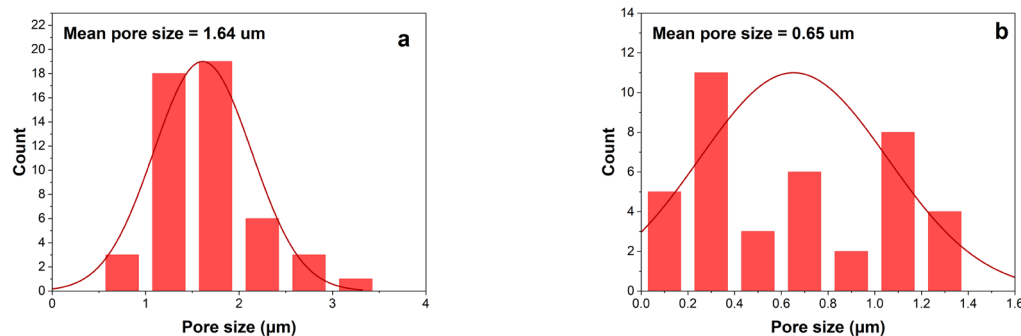


**Figure 5.** Pore size distribution of membrane at different concentration of CNT; (a) PVDF-0.5-wt% CNT; (b) PVDF-0.7-wt% CNT.

### 3.1.2. Porosity Test Results

The porosity of the fabricated membranes plays a crucial role in determining mass transfer performance and flux behaviour during membrane distillation processes. The porosity results are presented in Figure 6 for different types of membranes fabricated in this work, where bars show average values of replicates. The pristine PVDF membrane showed that porosity decreases by increasing PVDF concentration; membrane porosity decreased from 64% to 50% as PVDF concentration increased from 10% to 20%. This decrease in porosity is attributed to the higher polymer concentration that reduces the solvent–non-solvent exchange, and thus limits polymer chain mobility, which suppresses phase separation and pore formation. One study on polysulfone membranes demonstrated that higher polymer concentration resulted in denser structures with lower void fraction and reduced water permeation [33].

Membrane porosity is strongly influenced by several parameters, such as coagulation bath temperature and polymer molecular weight [34]. Moreover, the solvent's affinity for both the non-solvent and the polymer strongly governs pore formation; highly miscible solvents (e.g., DMF) promote faster demixing and higher porosity, whereas low compatible solvents (e.g., NMP) yield denser membranes [22].

The incorporation of a small amount of CNTs 0.3% to 0.7% into the 13%-PVDF matrix led to an increase in membrane porosity (Figure 6), which can be attributed to the enhanced phase separation during the non-solvent induced phase inversion process. It has been reported that CNT can act as nucleation sites within the polymer matrix, promoting faster demixing between the solvent and non-solvent phases and thereby creation of more voids and a higher overall porosity [24].

At higher CNT concentrations, the porosity of the PVDF membrane does not increase further. This behaviour is likely due to a significant increase in the viscosity of the dope solution, which suppresses the solvent–non-solvent exchange rate during phase the phase inversion process. Excess CNT tend to agglomerate because of the strong van der Waals interactions, forming clusters that block pore channels and hinder uniform pore formation [35]. At elevated CNT concentrations, aggregation occurs, which retards the demixing process and leads to a denser membrane structure with reduced void volume. Among the tested membranes, 13%-PVDF-CNT-0.5% can be considered the optimum, as it exhibits the highest porosity, provides a more favourable vapour transport pathway, and consequently achieve a higher flux.

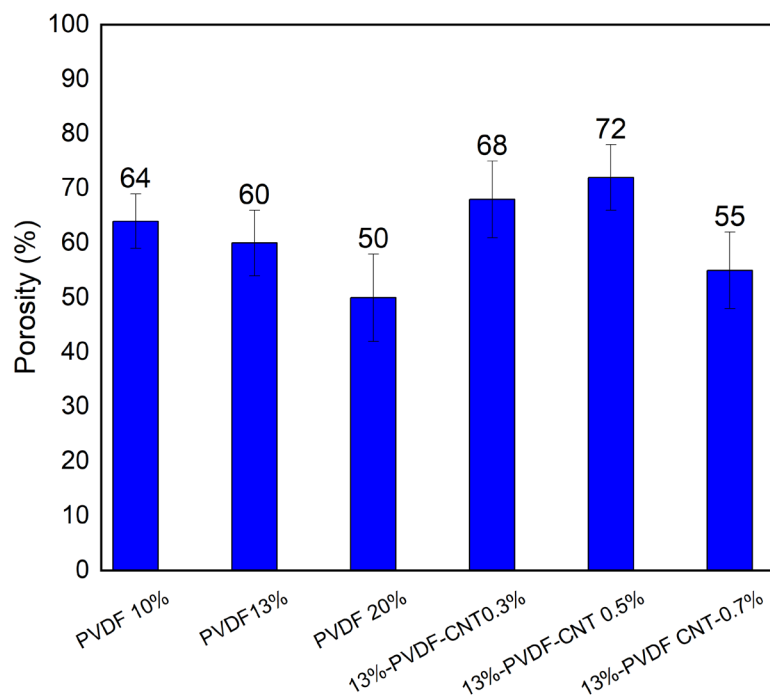


**Figure 6.** Porosity results for synthesized PVDF membranes at different concentrations and different concentrations of CNT nanoparticles.

### 3.1.3. Contact Angel Analysis

The contact angle reflects membrane surface wettability, which directly influences the performance of the membrane distillation process. A higher contact angle corresponds to a more hydrophobic surface, which is desirable in processes involving thermal desalination, as it helps prevent pore wetting and maintains a stable flux.

Figure 7 shows the contact angle of 13%-PVDF and 13%-PVDF-CNT-0.5% membranes developed in this work. The incorporation of carbon nanotubes (CNTs) into the membrane matrix significantly increases the water contact angle from 87° to 95.3°, indicating enhanced membrane hydrophobicity. This improvement is attributed to the inherent hydrophobic nature of CNTs and their ability to modify surface roughness and surface energy when well dispersed within the polymer matrix. Increased hydrophobicity is particularly beneficial for membrane distillation, as it improves resistance to membrane wettability and enhances long-term operational stability [36,37].

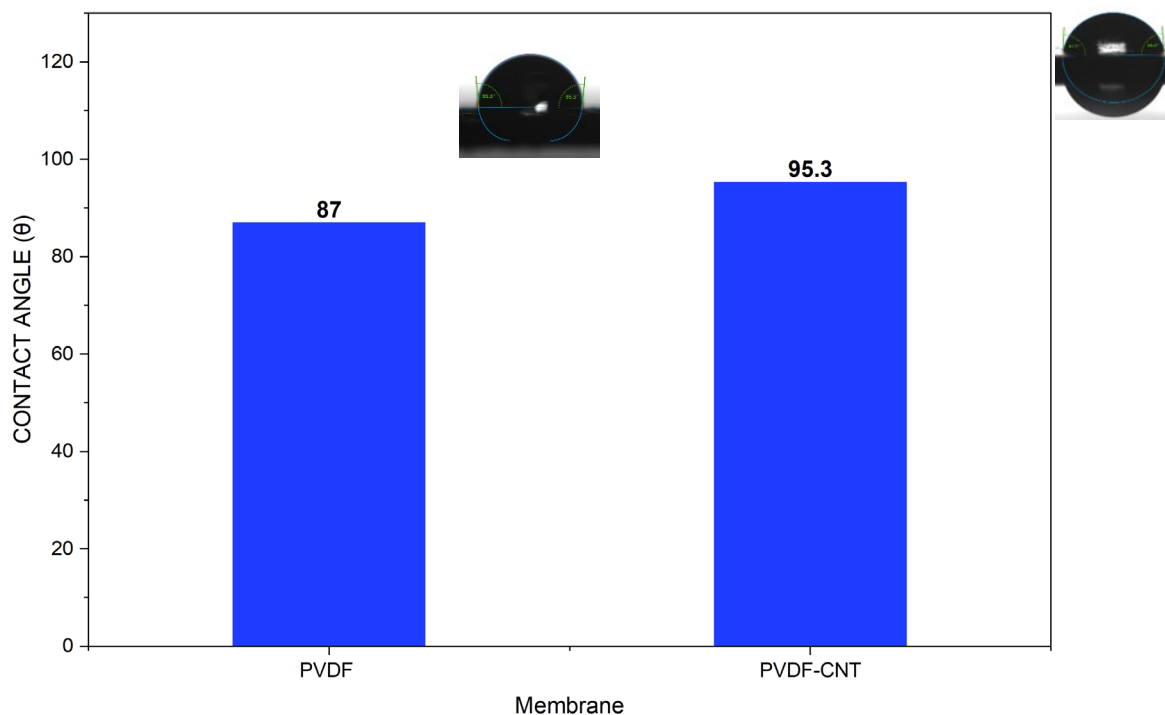


**Figure 7.** The contact angle for PVDF and PVDF-CNT membranes.

#### 3.1.4. FTIR Results

The Fourier transform infrared spectroscopy (FTIR) spectra (Thermo Scientific Id7 ATR) can provide evidence about successful surface modification of the PVDF membrane using tannic acid. Figure 8 shows peaks between 500 and 980  $\text{cm}^{-1}$  indicating presence of both  $\alpha$  (major) and  $\beta$ -phases (minor) of PVDF [38]. The peaks observed between 850 and 900  $\text{cm}^{-1}$  attributed to the  $\beta$ -phase whereas remaining represent the  $\alpha$ -phase, respectively [39][40]. Moreover, the peak around 1234  $\text{cm}^{-1}$  reveals the presence of  $\beta$ -phase [38]. A peak around 1400  $\text{cm}^{-1}$  represents the presence of  $\text{CH}_2$  [41]. In the pristine PVDF membrane, characteristic absorption peaks were observed at around 1070–1080  $\text{cm}^{-1}$  and 840–880  $\text{cm}^{-1}$ , corresponding to the C–F stretching and C–H bending vibrations of the PVDF backbone.

After incorporating CNTs into the PVDF, the FTIR signals slightly changed with a minor decrease in the intensity and a change of the positions for the wavenumbers between 700 and 860  $\text{cm}^{-1}$ , respectively. Since CNTs were present at very low concentrations relative to PVDF during the membrane fabrication, the signals corresponding to C–C, C–O and C–H are either very weak or not detectable [42,43].

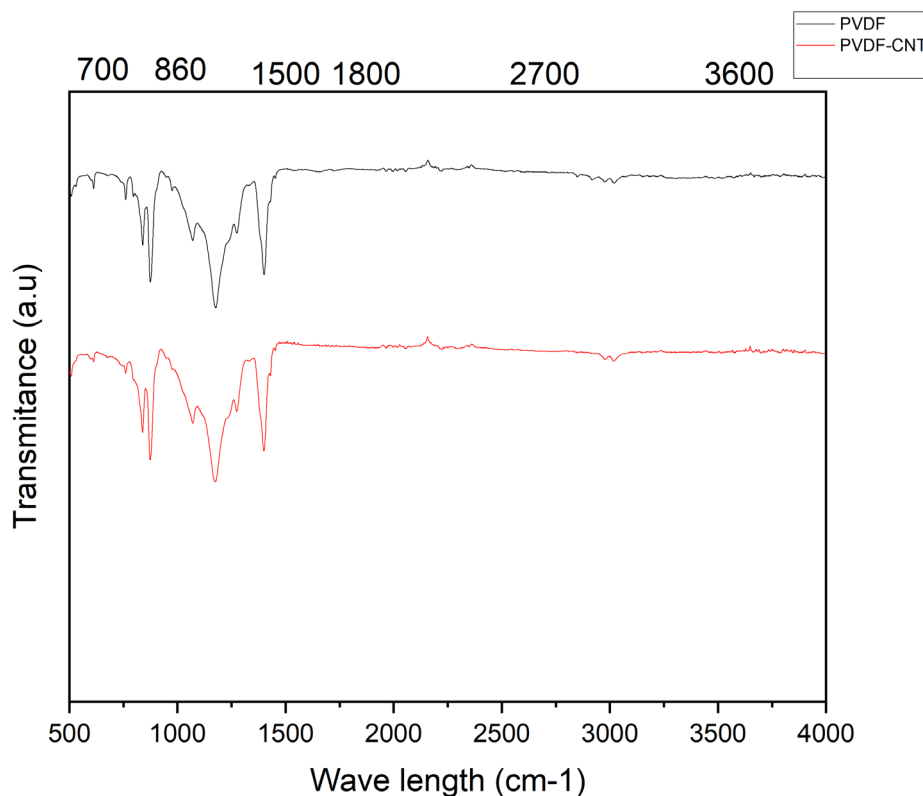


**Figure 8.** FTIR spectra for 13%-PVDF and 13%-PVDF-CNT-0.5% membranes.

### 3.1.5. Thermo Gravimetric Analysis

Thermogravimetric analysis (TGA) was performed in the presence of nitrogen using STA 6000 Perkin Elmer Thermal Analyzer. The temperature range for this analysis was set between 24 °C and 650 °C. Figure 9 shows the TGA results for the PVDF and PVDF-CNT membranes fabricated in this work. A major weight loss in the PVDF membrane was observed at around 420 °C, which corresponds to the breakdown of the  $-\text{CH}_2-\text{CF}_2-$  chains within the polymer backbone [44]. The PVDF polymer backbone remains thermally stable up to ~420 °C, which indicates that decomposition of the polymer does not occur below this temperature.

Decomposition of PVDF-CNT systems shifts to slightly higher temperatures, usually around 450 °C. This improvement is attributed to the strong interfacial interaction between the PVDF chains and the CNT surfaces, which restrict chain mobility and delay in thermal degradation [45]. Additionally, the residual mass (char yield) was significant at higher temperatures of 550 °C as compared to pristine PVDF. This indicates that CNT promote the formation of thermally stable carbonaceous structures that resists decomposition at elevated temperatures and enhance interfacial interactions, thereby reducing the degradation of PVDF chains. Additionally, CNT can act as a physical barrier, limiting polymer chain mobility and further promoting these thermally stable structures [41].

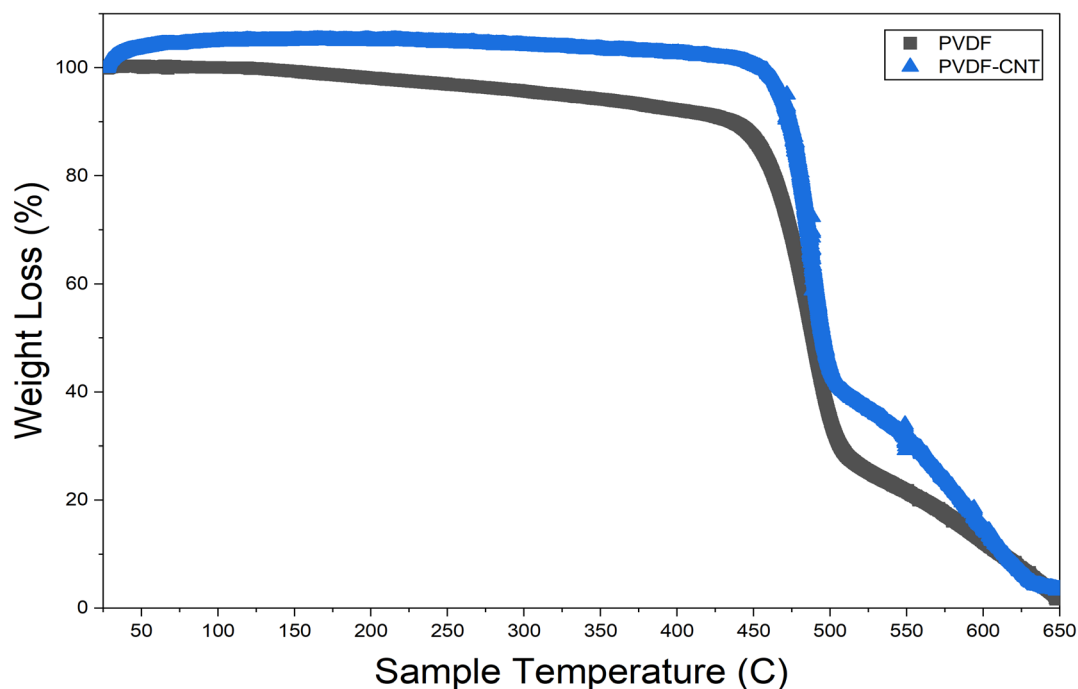


**Figure 9.** TGA analysis for 13%-PVDF and 13%-PVDF-CNT-0.5% membranes.

In 90. °C, TGA was performed to evaluate the thermal stability of the membrane material itself. The TGA determines temperature at which polymer starts to degrade. This ensured that the membrane can safely withstand long term heating, thermal cycling, and unexpected temperature fluctuations during the operation.

### 3.2. Membrane Performance

#### 3.2.1. Effect of Polymer Concentration on Flux and Rejection

The PVDF membranes were successfully fabricated using three different polymer concentrations: 10, 13, and 20 wt%. Each membrane was evaluated using a laboratory-scale direct contact membrane distillation (DCMD) cell with saline feed solution at 60 °C feed side temperature to assess flux and salt rejection performance. The experimental results showed distinct differences in performance depending on the PVDF concentration (Table 1).

**Table 1.** Membrane flux and rejection using PVDF at different concentration.

PVDF Conc	Flux				Salt Rejection			
	1st Run	2nd Run	Standard Error	Relative difference Percentage	1st Run	2nd Run	Standard Error	Relative difference Percentage
10%	10.2	8.15	1.025	22.34	98.9	99.2	0.15	0.30
13%	9.3	8	0.65	15.02	99	99.4	0.2	0.40
20%	7	6	0.5	15.38	99.99	100	0.005	0.01

The results shown in Table 1 indicate that, among membranes tested, the membrane prepared using 13 wt% PVDF demonstrated the most balanced overall performance. It results in high water flux of 8.65 LMH together with excellent salt rejection. The 13-wt% PVDF resulted in an optimal pore structure, providing sufficient porosity for vapor transport while maintaining structural stability and adequate hydrophobicity to prevent pore wetting.

The membrane fabricated using 10-wt% PVDF showed higher flux of 9.2 LMH compared to that of 13-wt%. Due to the lower polymer concentration, the resulting structure was highly porous and

mechanically weaker, leading to larger pore size and an increased risk of pore wetting [46]. Although this membrane exhibited relatively high initial flux, its salt rejection is lower, indicating that excessive porosity reduced the selective barrier properties required for effective MD operation. In contrast, membrane prepared using 20-wt% PVDF demonstrated lower flux of 6.5 LMH with 99% salt rejection. The higher polymer concentration revealed a denser structure with lower porosity and small pore size, which restricts vapor transport across the membrane.

The results presented in Table 1 emphasize that polymer concentration strongly influences membrane morphology and performance. Low PVDF concentrations may enhance permeability but compromise mechanical strength and durability, whereas higher concentrations improve structural stability at the cost of reduced flux. Thus, the 13 wt% PVDF membrane can be considered an optimal balance between permeability, selectivity, and mechanical strength for DCMD applications. This is consistent with a previous study, [43] which demonstrated that increasing polymer concentration in the dope solution results in a decrease in the flux [47]. This was attributed to the formation of a thicker and denser outer skin layer, underscoring the importance of optimizing polymer content for long-term membrane performance.

### 3.2.2. Effect of Nano Particles on Flux and Rejection

Three 13%-PVDF membranes were fabricated by incorporating different additives 0.5% each such as carbon nanotubes (CNT), graphene oxide (GO), and chitosan, into the polymer matrix. These additives are expected to enhance the structural and transport properties of the membranes. The three fabricated membranes were tested in a direct contact membrane distillation (DCMD) cell, at similar conditions and saline feed solution, to evaluate water flux and salt rejection. The results (Table 2) showed notable differences in flux depending on the additive used.

The CNT-modified membrane achieved the highest water flux of 10.5 LMH compared to the other samples. CNTs facilitated the formation of well-connected pore channels due to their one-dimensional tubular structure and improved the hydrophobic nature of the membrane [48]. This combination allowed efficient vapor transport while maintaining stability against wetting. Compared to the membrane without carbon nanotube (Figure 10), this result shows 21.4% increase in flux while salt rejection remains 99%.

**Table 2.** Membrane flux and rejection using 13-wt% PVDF with types of different additives 0.5% each.

13%-PVDF- ADDITIVE	Flux				Salt Rejection			
	1st Run	2nd Run	Standard Error	Relative difference Percentage	1st Run	2nd Run	Standard Error	Relative difference Percentage
<b>CNT</b>	10.8	10.2	0.3	5.71	99.3	99.9	0.3	0.60
<b>GO</b>	11	9	1	20	99.3	99.6	0.15	0.30
<b>CH</b>	8	11	1.5	31.57	98.9	99.2	0.15	0.30

The GO-modified membrane demonstrated a performance very close to that of the CNT membrane with a slightly lower flux, 10 LMH. The layered structure and oxygen-containing functional groups of GO may contribute to the improved dispersion in the polymer matrix and enhanced surface roughness, which aided water transport. However, compared to CNT, GO showed larger relative error in the measurements. This could be attributed to the manner in which the GO was dispersed. GO are pristine two-dimensional sheets exhibited a strong tendency to aggregate due to their large planar surface and van der Waals interactions, requiring longer times to achieve a reasonably uniform dispersion. Ultrasonic treatment can also cause fragmentation, defects, and changes in GO structure. Fragmented or defected GO can reduce uniformity in the membrane, leading to variations in flux measurements [49]. In contrast, CNT, with their one-dimensional tubular structure, were comparatively easier to disperse in NMP, as their smaller lateral dimension reduces restacking. Another investigation [50] reported that GO membranes have lower pore density and surface roughness, resulting in compromised performance compared to CNT membranes.

The chitosan-modified membrane showed the lowest flux among the three formulations, as illustrated in Table 2. The hydrophilic nature of chitosan caused partial pore wetting and reduced vapor transport efficiency, thereby limiting the overall membrane performance [51]. The relative error in the flux measurements could be attributed to differences in chitosan dispersion and dissolution behaviour. Chitosan is inherently hydrophilic and dissolve only in acidic aqueous solvents, such as dilute acetic acid [49,52] through protonation of its amino groups, while remaining insoluble in aprotic solvents like NMP. Ultrasonication can aid dispersion or accelerate dissolution in suitable solvents by breaking up aggregates and improving mixing; however, excessive sonication to achieve complete dispersion can cause polymer chain breakage, reduced molecular weight, and structural disorder [52]. These variations in solubility, dispersion uniformity, and potential polymer degradation result in a nonuniform membrane structure, leading to significant fluctuations in the measured flux.

### 3.2.3. Effect of CNT Concentration on Flux and Rejection

To investigate the influence of CNT concentration on membrane performance, three 13%-PVDF membranes were prepared using CNT concentrations of 0.3, 0.5, and 0.7 wt%, respectively. Due to their unique one-dimensional structure, the incorporation of CNTs was expected to enhance pore connectivity, mechanical strength, and vapor transport. All membranes were tested under the same DCMD conditions and same saline feed solution, and their flux and salt rejection measurements were compared. The results are shown in Table 3.

The membrane with 0.5 wt% CNT exhibited the highest water flux of 11.5 LMH, while maintaining excellent salt rejection. At this concentration, the CNTs were well-dispersed in the polymer matrix, forming a more interconnected pore network that facilitates efficient vapor transport. Moreover, the moderate CNT loading improved hydrophobicity without causing pore blockage.

**Table 3.** Membrane flux and rejection using 13-wt% PVDF at different concentrations of CNT.

13%-PVDF-CNT		Flux			Salt Rejection			
CNT Conc	1st Run	2nd Run	Standard Error	Relative difference Percentage	1st Run	2nd Run	Standard Error	Relative difference Percentage
0.3%	12	9	1.5	28.57	98	99	0.5	1.01
0.5%	11	12	0.5	8.69	97.9	99.5	0.8	1.62
0.7%	10.5	11.5	0.5	9.09	97.5	99.3	0.9	1.82

The 0.3 wt% CNT membrane exhibited the lowest flux among the three membrane formulations. At such a low loading, the CNTs were insufficient to significantly alter the pore structure or enhance vapor transport pathways, resulting in performance similar to that of the pristine PVDF membrane with only limited flux improvement. This suggests that a minimum CNT concentration is necessary to achieve noticeable enhancements. A similar trend was reported by another study, where increasing the CNT content from 0.2% to 0.3% led to an improved flux [53].

The 0.7-wt% CNT membrane showed intermediate performance, with flux higher than that of the 0.3-wt% CNT membrane but lower than that of the 0.5-wt% membrane. The reduced flux is attributed to CNT agglomeration at higher loadings, which partially blocked pores and limited effective vapor transport channels. Although mechanical reinforcement and salt rejection remained satisfactory, the excessive CNT content hindered further flux improvement. Comparing these results with Figure 10, the addition of 0.3%, 0.5%, and 0.7% CNT led to flux increase of 21.4%, 32.9%, 27.2%, respectively, relative to the pristine PVDF membrane.

## 4. Conclusions

This study systematically evaluated the effects of polymer concentration and nanofiller incorporation on PVDF membrane performance. Among the formulations, 13-wt% PVDF was identified as optimal, offering improved morphology and overall performance. Comparative testing of CNT, GO, and chitosan showed that CNTs provided the greatest enhancement, with 0.5-wt% CNT yielding uniform dispersion, improved pore structure, enhanced mass transport, and superior separation efficiency. Lower or higher CNT loadings reduced performance, highlighting 0.5-wt% as the optimal nanofiller content for advanced membrane applications.

**Author Contributions:** Conceptualization, N.A.D., N.A.J., and M.Q.; Methodology, S.F.S., F.S.M., M.Q.; Validation, S.F.S., S.A.-A., and F.S.M.; Formal analysis, S.F.S., N.A.D., N.A.J., M.Q., S.A.-A., and F.S.M.; Investigation, S.F.S., N.A.D., N.A.J., M.Q., S.A.-A., and F.S.M.; Writing—original draft, F.S.M.; Writing—review & editing, S.F.S., S.A.-A., F.S.M.; Supervision, N.A.D., N.A.J., S.A.-A., and F.S.M.; Funding acquisition, N.A.J. All authors have read and agreed to the published version of the manuscript.

**Funding:** This research was funded by the Office of Research at the American University of Sharjah (FRG24-C-E68).

**Institutional Review Board Statement:** Not applicable.

**Informed Consent Statement:** Not applicable.

**Data Availability Statement:** The raw data supporting the conclusions of this article will be made available by the authors on request.

**Acknowledgments:** The authors gratefully acknowledge the support of Dr. Amani Al-Othman for her guidance and for providing access to the phase-inversion apparatus used in membrane fabrication. The financial support of the Office of Research at AUS is also acknowledged.

**Conflicts of Interest:** The authors declare no conflicts of interest.

## References

1. Jayaswal, K.; Sahu, V.; Gurjar, B.R. Water Pollution, Human Health and Remediation. In *Water remediation*; Springer, 2017; pp. 11–27.
2. Mishra, R.K. Fresh Water Availability and Its Global Challenge. *British Journal of Multidisciplinary and Advanced Studies* **2023**, *4*, 1–78.
3. Aliyu, U.M.; Rathilal, S.; Isa, Y.M. Membrane Desalination Technologies in Water Treatment: A Review. *Water Pract. Technol.* **2018**, *13*, 738–752.
4. Abdelrasoul, A.; Doan, H.; Lohi, A. Sustainable Water Technology and Water-Energy. Biomimetic and bioinspired membranes for new frontiers in sustainable water treatment technology **2017**, *1*.
5. Wu, J.; Zhang, Y.; Wang, J.; Zheng, X.; Chen, Y. Municipal Wastewater Reclamation and Reuse Using Membrane-Based Technologies: A Review. *Desalination Water Treat.* **2021**, *224*, 65–82.
6. Kucera, J. *Reverse Osmosis*; John Wiley & Sons, 2023; ISBN 1119724740.
7. Souhaimi, M.K.; Khayet, M.; Matsuura, T. Membrane Distillation: Principles and Applications. **2011**.
8. Chin, J.Y.; Ahmad, A.L.; Low, S.C. Anti-Wetting Membrane Distillation to Treat High Salinity Wastewater. *Journal of Membrane Science and Research* **2020**, *6*, 401–415.
9. Chen, L.; Xu, P.; Wang, H. Interplay of the Factors Affecting Water Flux and Salt Rejection in Membrane Distillation: A State-of-the-Art Critical Review. *Water (Basel)*. **2020**, *12*, 2841.
10. Sinha Ray, S.; Singh Bakshi, H.; Dangayach, R.; Singh, R.; Deb, C.K.; Ganesapillai, M.; Chen, S.-S.; Purkait, M.K. Recent Developments in Nanomaterials-Modified Membranes for Improved Membrane Distillation Performance. *Membranes (Basel)*. **2020**, *10*, 140.

11. Nasib, A.M.; Hatim, I.; Jullok, N.; Alamery, H.R. Morphological Properties of Poly (Vinylidene Fluoride-Cotetrafluoroethylene Membrane): Effect of Solvents and Polymer Concentrations. *Malaysian Journal of Analytical Sciences* **2017**, *21*, 356–364.
12. Mousavi, S.M.; Raveshiyan, S.; Amini, Y.; Zadhoush, A. A Critical Review with Emphasis on the Rheological Behavior and Properties of Polymer Solutions and Their Role in Membrane Formation, Morphology, and Performance. *Adv. Colloid Interface Sci.* **2023**, *319*, 102986.
13. Nthunya, L.N.; Gutierrez, L.; Verliefe, A.R.; Mhlanga, S.D. Enhanced Flux in Direct Contact Membrane Distillation Using Superhydrophobic PVDF Nanofibre Membranes Embedded with Organically Modified SiO<sub>2</sub> Nanoparticles. *Journal of Chemical Technology & Biotechnology* **2019**, *94*, 2826–2837.
14. Sawant, S.R.; Kalla, S.; Murthy, Z.V.P. Nanomaterial–Incorporated Membrane Distillation Membranes: Characteristics, Fabrication Techniques, and Applications. *Chem. Eng. Technol.* **2023**, *46*, 1982–2006.
15. Dong, X.; Lu, D.; Harris, T.A.L.; Escobar, I.C. Polymers and Solvents Used in Membrane Fabrication: A Review Focusing on Sustainable Membrane Development. *Membranes (Basel)*. **2021**, *11*, 309.
16. Fateev, N.; Velmozhin, K.; Danilkin, A.; Kotyukova, A.; Yasneva, T.; Ivanov, M.; Kagramanov, G. Enhanced Filtration Performance of Hollow Fiber PVDF Membranes with Selective Pore Size Control via Modified NIPS Method. *Membrane Science International* **2025**, *4*, 1–11.
17. Dong, X.; Lu, D.; Harris, T.A.L.; Escobar, I.C. Polymers and Solvents Used in Membrane Fabrication: A Review Focusing on Sustainable Membrane Development. *Membranes (Basel)*. **2021**, *11*, 309.
18. El Fadil, A. Upscaling Solvent-Tolerant Nanofiltration: Criteria, Water/Solvent Permeance Analysis, and Synthesis of Epoxy-Based Membranes. **2024**.
19. Ekambaram, K.; Doraisamy, M. Study on the Fabrication, Characterization and Performance of PVDF/Calcium Stearate Composite Nanofiltration Membranes. *Desalination* **2016**, *385*, 24–38.
20. Ajari, H.; Zrelli, A.; Chaouachi, B.; Pontié, M. Preparation and Characterization of Hydrophobic Flat Sheet Membranes Based on a Recycled Polymer. *International Polymer Processing* **2019**, *34*, 376–382.
21. Tian, E.; Wang, X.; Wang, X.; Ren, Y.; Zhao, Y.; An, X. Preparation and Characterization of Thin-Film Nanocomposite Membrane with High Flux and Antibacterial Performance for Forward Osmosis. *Ind. Eng. Chem. Res.* **2018**, *58*, 897–907.
22. Thilagashanthi, T.; Gunasekaran, K.; Satyanarayanan, K.S. Microstructural Pore Analysis Using SEM and ImageJ on the Absorption of Treated Coconut Shell Aggregate. *J. Clean. Prod.* **2021**, *324*, 129217.
23. Baroud, T.N. Tuning PVDF Membrane Porosity and Wettability Resistance via Varying Substrate Morphology for the Desalination of Highly Saline Water. *Membranes (Basel)*. **2023**, *13*, 395.
24. Islam, M.D.; Uddin, F.J.; Rashid, T.U.; Shahruzzaman, M. Cellulose Acetate-Based Membrane for Wastewater Treatment—A State-of-the-Art Review. *Mater. Adv.* **2023**, *4*, 4054–4102.
25. Baroud, T.N. Tuning PVDF Membrane Porosity and Wettability Resistance via Varying Substrate Morphology for the Desalination of Highly Saline Water. *Membranes (Basel)*. **2023**, *13*, 395.
26. Bouleklab, M.C.; Hamamda, S.; Naoui, Y.; Nedilko, S.; Avramenko, T.; Ivanenko, K.; Revo, S.; Teselko, P.; Strelchuk, V.; Nikolenko, A. Influence of the Multiwall Carbon Nanotubes on the Thermal Properties of the Fe–Cu Nanocomposites. *J. Alloys Compd.* **2020**, *816*, 152525.
27. Liu, M.; Chen, D.; Xu, Z.; Wei, Y.; Tong, M. Effects of Nucleating Agents on the Morphologies and Performances of Poly (Vinylidene Fluoride) Microporous Membranes via Thermally Induced Phase Separation. *J. Appl. Polym. Sci.* **2013**, *128*, 836–844.
28. Udoh, C.E.; Garbin, V.; Cabral, J.T. Microporous Polymer Particles via Phase Inversion in Microfluidics: Impact of Nonsolvent Quality. *Langmuir* **2016**, *32*, 8131–8140.
29. Islam, M.D.; Uddin, F.J.; Rashid, T.U.; Shahruzzaman, M. Cellulose Acetate-Based Membrane for Wastewater Treatment—A State-of-the-Art Review. *Mater. Adv.* **2023**, *4*, 4054–4102.
30. Akbari, A.; Hamadian, M.; Jabbari, V.; Lehi, A.Y.; Bojaran, M. Influence of PVDF Concentration on the Morphology, Surface Roughness, Crystalline Structure, and Filtration Separation Properties of Semicrystalline Phase Inversion Polymeric Membranes. *Desalination Water Treat.* **2012**, *46*, 96–106.
31. Chazot, C.A.C.; Hart, A.J. Understanding and Control of Interactions between Carbon Nanotubes and Polymers for Manufacturing of High-Performance Composite Materials. *Compos. Sci. Technol.* **2019**, *183*, 107795.

32. Sun, X.; Shiraz, H.; Wong, R.; Zhang, J.; Liu, J.; Lu, J.; Meng, N. Enhancing the Performance of PVDF/GO Ultrafiltration Membrane via Improving the Dispersion of GO with Homogeniser. *Membranes (Basel)*. **2022**, *12*, 1268.
33. Arahman, N.; Sari, W.P.; Sari, I.M.; Rosnelly, C.M.; Mulyati, S.; Fahrina, A.; Bilad, M.R.; Gunawan, P.; Pasaoglu, M.E.; Teber, O.O. The Effectiveness of Polyvinylidene Fluoride Membranes Modified with Poloxamer and Single/Multi-Walled Carbon Nanotubes for Lactalbumin Purification. *ChemEngineering* **2022**, *6*, 88.
34. Tiron, L.G.; Pintilie, S.C.; Lazar, A.L.; Vlad, M.; Balta, S.; Bodor, M. Influence of Polymer Concentration on Membrane Performance in Wastewater Treatment. *Mater. Plast* **2018**, *55*, 95–98.
35. Rubel, R.I.; Ali, M.H.; Jafor, M.A.; Alam, M.M. Carbon Nanotubes Agglomeration in Reinforced Composites: A Review. *AIMS Mater. Sci.* **2019**, *6*, 756–780.
36. Omar, N.M.A.; Othman, M.H.D.; Tai, Z.S.; Kurniawan, T.A.; Puteh, M.H.; Jaafar, J.; Rahman, M.A.; Bakar, S.A.; Abdullah, H. A Review of Superhydrophobic and Omniphobic Membranes as Innovative Solutions for Enhancing Water Desalination Performance through Membrane Distillation. *Surfaces and Interfaces* **2024**, *46*, 104035.
37. Swaminathan, M.; Swaminathan, G. An Insight into Enhanced Membrane Hydrophobicity Using Silane Functionalization for Effective Membrane Distillation. *Separation & Purification Reviews* **2025**, *54*, 220–240.
38. Cai, X.; Lei, T.; Sun, D.; Lin, L. A Critical Analysis of the  $\alpha$ ,  $\beta$  and  $\gamma$  Phases in Poly (Vinylidene Fluoride) Using FTIR. *RSC Adv.* **2017**, *7*, 15382–15389.
39. Wang, S.; Liang, S.; Liang, P.; Zhang, X.; Sun, J.; Wu, S.; Huang, X. In-Situ Combined Dual-Layer CNT/PVDF Membrane for Electrically-Enhanced Fouling Resistance. *J. Memb. Sci.* **2015**, *491*, 37–44, doi:https://doi.org/10.1016/j.memsci.2015.05.014.
40. Mishra, S.; Kumaran, K.T.; Sivakumaran, R.; Pandian, S.P.; Kundu, S. Synthesis of PVDF/CNT and Their Functionalized Composites for Studying Their Electrical Properties to Analyze Their Applicability in Actuation & Sensing. *Colloids Surf. A Physicochem. Eng. Asp.* **2016**, *509*, 684–696, doi:https://doi.org/10.1016/j.colsurfa.2016.09.007.
41. Behera, S.A.; Nanda, B.; Achary, P.G.R. PVDF-Based Functional Composites for Efficient Degradation of Methylene Blue. *Discover Applied Sciences* **2025**, *7*, 927, doi:10.1007/s42452-025-07470-8.
42. Yang, J.; Xiao, Y.; Yang, C.; Li, S.; Qi, X.; Wang, Y. Multifunctional Poly(Vinylidene Fluoride) Nanocomposites via Incorporation of Ionic Liquid Coated Carbon Nanotubes. *Eur. Polym. J.* **2018**, *98*, 375–383, doi:https://doi.org/10.1016/j.eurpolymj.2017.11.037.
43. Zhang, W.; Zhang, Z.; Yang, J.; Huang, T.; Zhang, N.; Zheng, X.; Wang, Y.; Zhou, Z. Largely Enhanced Thermal Conductivity of Poly(Vinylidene Fluoride)/Carbon Nanotube Composites Achieved by Adding Graphene Oxide. *Carbon N. Y.* **2015**, *90*, 242–254, doi:https://doi.org/10.1016/j.carbon.2015.04.040.
44. de Jesus Silva, A.J.; Contreras, M.M.; Nascimento, C.R.; da Costa, M.F. Kinetics of Thermal Degradation and Lifetime Study of Poly (Vinylidene Fluoride)(PVDF) Subjected to Bioethanol Fuel Accelerated Aging. *Heliyon* **2020**, *6*.
45. Rehman, Z.U.; Ahmad, S.; Ullah, H.; Alqarni, S.A.; Yao, S.; Khan, K.A.; Zaki, M.E.A. Thermal and Electrical Properties of PVDF Modified Co 3 O 4 Functionalized MWCNTs. *RSC Adv.* **2025**, *15*, 8740–8749.
46. Fomin, S.; Shirokova, E.; Kraeva, I.; Tolstobrov, I.; Bushuev, A.; Yuzhanin, K.; Ananchenko, B.; Vetcher, A.A.; Iordanskii, A. Effect of Polyvinylidene Fluoride Membrane Production Conditions on Its Structure and Performance Characteristics. *Polymers (Basel)*. **2022**, *14*, 5283.
47. Ghasem, N.; Al-Marzouqi, M.; Duidar, A. Effect of PVDF Concentration on the Morphology and Performance of Hollow Fiber Membrane Employed as Gas–Liquid Membrane Contactor for CO<sub>2</sub> Absorption. *Sep. Purif. Technol.* **2012**, *98*, 174–185.
48. Francis, L.; Hilal, N. Electrosprayed CNTs on Electrospun PVDF-Co-HFP Membrane for Robust Membrane Distillation. *Nanomaterials* **2022**, *12*, 4331.
49. Zhang, B.; Chen, T. Study of Ultrasonic Dispersion of Graphene Nanoplatelets. *Materials* **2019**, *12*, 1757.
50. Zhao, Y.; Xu, Z.; Shan, M.; Min, C.; Zhou, B.; Li, Y.; Li, B.; Liu, L.; Qian, X. Effect of Graphite Oxide and Multi-Walled Carbon Nanotubes on the Microstructure and Performance of PVDF Membranes. *Sep. Purif. Technol.* **2013**, *103*, 78–83.

51. Machodi, M.J.; Daramola, M.O. Synthesis of PES and PES/Chitosan Membranes for Synthetic Acid Mine Drainage Treatment. *Water SA* **2020**, *46*, 114–122.
52. Tang, E.S.K.; Huang, M.; Lim, L.Y. Ultrasonication of Chitosan and Chitosan Nanoparticles. *Int. J. Pharm.* **2003**, *265*, 103–114.
53. Silva, T.L.S.; Morales-Torres, S.; Figueiredo, J.L.; Silva, A.M.T. Multi-Walled Carbon Nanotube/PVDF Blended Membranes with Sponge-and Finger-like Pores for Direct Contact Membrane Distillation. *Desalination* **2015**, *357*, 233–245.

**Disclaimer/Publisher's Note:** The statements, opinions and data contained in all publications are solely those of the individual author(s) and contributor(s) and not of MDPI and/or the editor(s). MDPI and/or the editor(s) disclaim responsibility for any injury to people or property resulting from any ideas, methods, instructions or products referred to in the content.